Investigation of the Impact of the Electric Field Variability on the Joule Heating, Neutral Temperature and Density with a New Empirical Model

Yue Deng, Astrid Maute, Arthur D. Richmond and Ray G. Roble

High Altitude Observatory, National Center for the Atmospheric Research,

Boulder Colorado, U.S.A.

Yue Deng (e-mail: ydeng@ucar.edu), Astrid Maute (e-mail: maute@ucar.edu), Arthur D. Richmond (e-mail: richmond@ucar.edu), Ray G. Roble (e-mail: roble@ucar.edu).

Abstract.

A new quantitative empirical model of the high-latitude forcing of the thermosphere, which is the first empirical model with an electric field variability component consistent with the average electric field, is used with the NCAR-TIEGCM to investigate the influence of the electric field variability on the Joule heating, neutral temperature and density. The electric field variability increases the Joule heating by more than 100%, and significantly improves the agreement between the total Joule heating and Poynting flux, while the horizontal distributions of the height-integrated Joule heating and the Poynting flux have some detailed differences in the polar cap and nightside regions. Including the electric field variability into the energy calculation results in significant changes in the neutral temperature and density. At 400 km, it causes a 120 K polar average temperature increase and the corresponding percentage difference of density is close to 30%.

1. Introduction

The thermosphere/ionosphere is forced by solar EUV radiation, high-latitude electrodynamics, particle precipitation and waves propagating from the lower atmosphere. In the polar region, field-aligned currents from the magnetosphere are closed by ionospheric currents, and bring a significant amount of energy into the thermosphere/ionosphere. The energy is highly variable with the geomagnetic conditions and can cause global scale disturbances in the thermosphere/ionosphere during a storm period. However, this energy has usually been underestimated when the general circulation models (GCMs) are driven by climatological convection models. For example, *Emery et al.* [1999] needed to mutiply the calculated Joule heating by 2.5 in order to reproduce observed thermospheric responses. This insufficient energy is attributed to the neglect of the contribution of electric field variability to the Joule heating [*Codrescu et al.*, 1995]. Using the ion drift data from the Millstone Hill radar, *Codrescu et al.* [1995] reported that the electric field variability has a similar magnitude as the average electric field. Indeed, subsequent studies [*Codrescu et al.*, 2000; *Crowley and Hackert*, 2001; *Matsuo et al.*, 2003; *Matsuo and Richmond*, 2008] showed that the electric field variability can be comparable to or even larger than the average electric field.

While the significance of electric field variability to the Joule heating has been recognized, we still face a big challenge to implement the electric field variability in the GCMs appropriately and conveniently. Empirical models have been developed to characterize the auroral precipitation [*Hardy et al.*, 1987; *Fuller-Rowell and Evans*, 1987] and high-latitude electric potential [*Foster et al.*, 1986; *Ruohoniemi and Greenwald*, 1996; *Ridley et al.*, 2000; *Weimer*, 2001; *Weimer*, 2005] under various geophysical conditions, which are often used to force GCMs.

However, the models of the electric potential represent only the statistical average of the vector field $\langle \mathbf{E} \rangle$, and the difference between $\mathbf{E}$ and $\langle \mathbf{E} \rangle$, called "residual electric field", has been ignored. To quantify the Joule heating associated with the residual electric field in a way consistent with the empirical model of electric potential used as GCM inputs, a new empirical model with an electric field variability component has been developed and coupled with the NCAR-TIEGCM [*Roble et al.*, 1988; *Richmond*, 1992], which supplies a more realistic way to include electric field variability in the energy estimation than through ad hoc increases to the Joule heating. In this paper, we compare the thermospheric responses to the Joule heating calculated either from an empirical model of electric potential, or from both this potential and the empirical model of electric field variability. The resulting energy inputs then have been validated with the empirical model of Poynting flux. Including the electric field variability significantly improves consistency between the Joule heating and Poynting flux, and the corresponding neutral temperature and density increase substantially.

2. Empirical Model of the High Latitude Forcing

Dynamic Explorer 2 (DE-2) is one of only a few spacecraft that measured simultaneously the electric and magnetic fields, ion velocities, and particle precipitation at low-Earth orbit. By analyzing observations from the DE-2 spacecraft, a comprehensive, mutually consistent model of high-latitude thermospheric forcing has been developed and will be detailed in a separate paper. Totally, 2895 satellite passes during August 1981-March 1983 have been used in the process. The cross-track ion drift measurements are from the Ion Drift Meter (IDM), the along-track ion drift measurements are from the Retarding Potential Analyzer (RPA), and the magnetic field measurements are from the Fluxgate Magnetometer (MAGB). The electric field $\vec{E}$ is calculated

as $-\vec{V} \times \vec{B}$, where $\vec{V}$ is the ion velocity in the Earth frame and $\vec{B}$ is the geomagnetic field. A magnetic perturbation field $\Delta\vec{B}$ is obtained by subtracting a main-field model from the observations, and then correcting for spacecraft attitude uncertainties by subtracting a straight-line baseline that goes to zero at $\pm 45^{\circ}$ magnetic latitude. The observations were fitted, at each magnetic latitude, to analytical functions of magnetic local time (MLT), dipole tilt angle with respect to the plane normal to the Sun-Earth line, and strength and clock angle of the interplanetary magnetic field (IMF) obtained from the ACE satellite measurements. Currently, the empirical model includes four components: electric potential, magnetic potential, electric field variability and Poynting flux. A consistent auroral particle precipitation model will be developed in the future through analyzing the ion / electron energy flux data from the Low Altitude Plasma Instrument (LAPI).

The resultant electric and magnetic potentials from the new empirical model are generally consistent with those of *Weimer* [2005], which were derived from the along-track components of electric and magnetic fields. The downward Poynting flux S_{down} at the top of the thermosphere is estimated using the combined ion-drift and magnetometer data. In this model, the Poynting flux is calculated from the point measurements of electric field and magnetic field data from the DE-2 satellite, and is then fitted to analytical funtions in a similar manner as the electric and magnetic potentials. The resultant model is similar to the average of the product of $\mathbf{E}$ and $\triangle\mathbf{B}$ ($\frac{<\mathbf{E}\times\triangle\mathbf{B}>}{\mu_0}$), which at some level includes the contribution of the electric field variability. In contrast, the *Weimer* [2005] model calculates the Poynting flux from the product of average $\mathbf{E}$ and $\triangle\mathbf{B}$ as $\frac{<\mathbf{E}>\times<\triangle\mathbf{B}>}{\mu_0}$. Our model of electric field variability is the root mean square (RMS)

of the difference between the DE-2 observations E^{DE2} and the electric field from the model E^{model} of electric potential:

$$\sigma(E) = \sqrt{\frac{\sum_{i=1}^{N}(E_i^{DE2} - E_i^{model})^2}{N}}, \quad (1)$$

where the subscript i is for an individual measurements, N is number of measurements, σ is calculated separately for the eastward and poleward components of $\vec{E}$. Since the electric field variability just represents the difference between the DE-2 observation and empirical average model, it includes both small- and large-scale spatial variations, as well as temporal variations. The patterns and magnitudes of the electric-field variability, not shown here, are comparable with those shown by *Matsuo et al.* [2003]. This is the first empirical model in the community which includes a electric field variability component consistent with the average electric field.

3. Results

To investigate the importance of electric field variability to the Joule heating, we have coupled the new high-latitude forcing model into the TIEGCM. Figure 1a shows the distribution of the altitude-integrated Joule heating from an equinox simulation in the northern hemisphere, when the empirical electric potential from the new forcing model has been used to drive the ion drift. The IMF conditions are $B_y = 0$ and $B_z = -5nT$. The hemispheric power of precipitating auroral particles is 30 GW, and $F_{10.7}$ is $150\times10^{-22}W/m^2Hz$. Figure 1b is the same as Figure 1a, except that the electric field variability from the empirical forcing model has also been implemented in the TIEGCM. The electric field variation is used by alternating the sign of the electric field standard deviation from the model for a given point at every time step in both the north-south and east-west directions. Comparison between Figures 1a and 1b shows that the

electric field variability increases the Joule heating significantly. For example, the maximum at dawn and dusk increases from 0.009 to 0.018 W/m^2. To derive Joule heating from GCMs requires accurate information about the instantaneous patterns of ionospheric conductivities and thermospheric winds. The estimates of height-integrated Joule heating need to be calibrated against techniques less subject to bias, like the estimation of Poynting flux. Figure 1c shows the Poynting flux at the top of the thermosphere from the new empirical model. Both Figures 1b and 1c show dawn and dusk peaks with similar magnitudes, and a large energy flux in the dayside cusp region. But the Poynting flux is larger in the polar cap and smaller on the night side than the Joule heating calculated with the average electric field and electric field variability.

Figure 2 shows the hemispherically integrated Joule heating from TIEGCM simulations and Poynting flux from the new empirical model in different seasons. The difference between the green columns and dark blue columns is more than 100%, which indicates the electric field variability has a comparable contribution to the Joule heating as the average electric field. The light blue columns represent the integrated Poynting flux from the new empirical model. Clearly, the calculated Joule heating with the average electric field and electric field variability is much closer to the Poynting flux than that only with the average electric field. Generally, the electric field variability strongly improves the agreement between Joule heating and Poynting flux. In summer and winter seasons, the calculated total Joule heating is larger than the Poynting flux, which is not physical because the generation of wind kinetic energy by the Lorentz force of the current has a small positive value (not shown), and Poynting flux is equal to the sum of Joule heating and Kinetic-energy generation [e.g., *Thayer and Vickrey*, 1992]. This may be caused in part by inconsistency between the conductivity and the electric field when the Joule heating

is calculated in the TIEGCM. In the future, the empirical model will also include a consistent particle precipitation part, which may help to make the patterns of conductivity and electric field more consistent. The Joule heating calculated with the average electric field in summer is larger than that in winter, which is similar to the seasonal variation of the Joule heating shown in *Weimer* [2005]. *Matsuo et al.* [2003] presented a clear seasonal dependence of the electric field variability, with a maximum in winter and minimum in summer. However, in our study the energy contribution of electric field variability, which is indicated by the difference between the dark blue and green columns in Figure 2, has no clear seasonal dependence. This is because the conductance is largest in summer and smallest in winter, which is opposite to the seasonal variation of electric field variability.

Figure 3a shows the polar average (poleward $47.5°$) thermospheric temperature profiles with different high-latitude energy inputs in the equinox season. The difference between the case in which only the average electric field is used in the Joule heating calculation (black) and the case in which both the average electric field and electric field variability are used (red) is close to 120 K above 300 km altitude. *Fesen et al.* [1997] reported that the TIEGCM simulated neutral temperature is 100-200 K lower than the Millistone Hill observation at 300 km for the January 1993 campaign and it was proposed that the discrepancy was due to the underestimate of Joule heating caused by the electric field variability. The similarity between the temperature difference shown in this study and that presented in *Fesen et al.* [1997] indicates that including the electric field variability will improve the agreement between observation and simulation. Figure 3b shows the distribution of temperature difference between the two cases with and without electric field variability at 400 km altitude. The temperature difference is positive in the whole

polar region, and the maximum difference is 250 K in the dawnside and the minimum is close to 62 K at lower latitudes. Interestingly, there is no clear relation between the patterns of temperature and height-integrated heating, due to the fact that dynamics has a major influence on the temperature. As a reference, the blue line in Figure 3a shows the temperature profile obtained when the Poynting flux from the new empirical model has been used to specify the energy input from the magnetosphere. Since the Poynting flux model contains no information about the altitudes where the electromagnetic energy is deposited, the energy has been distributed vertically as heat according to the Pederson conductivity [*Deng et al.*, 2008]. In Figure 3a, the red line is closer to the blue line than to the black line, and the difference between the red and blue lines is close to 50 K above 300 km, which is related to the total energy difference between Joule heating and Poynting flux shown in Figure 2.

Figure 4a shows the density percentage difference compared with the case in which the Joule heating is calculated with the average electric field. When the Joule heating is calculated including the electric field variability (red), the polar-average density increases by 30% at 400 km altitude. Figure 4b shows that the maximum density percentage difference goes to more than 70% and the minimum is above 15% at 400 km. The density difference is significant and comparable with the density disturbance observed by CHAMP during a moderate geomagnetic storm [*Liu et al.*, 2005]. Clearly, the variations of density and temperature have different patterns. One possible reason is that Figure 3b shows the value difference of temperature and Figure 4b shows the percentage difference of density. Meanwhile, the horizontal convection, as well as the vertical atmospheric expansion and contraction caused by the variation of temperature, can change the density distribution significantly .

4. Summary and Conclusion

The significance of electric field variability to the Joule heating has been pointed out by *Codrescu et al.* [1995] and subsequent studies, but it is still very challenging to include the electric field variability in the GCMs appropriately and conveniently. A new quantitative empirical model of the high-latitude forcing of the thermosphere, including electric potential, electric field variability and Poynting flux, is coupled with the NCAR-TIEGCM to investigate the influence of the electric field variability on the Joule heating, neutral temperature and density.

In the TIEGCM simulations, the Joule heating has been calculated with and without the electric field variability. The integrated Joule heating has been validated with the Poynting flux from the empirical model. The analysis reveals that the electric field variability increases the Joule heating by more than 100%, and significantly improves the consistency between the Joule heating and Poynting flux, while their horizontal distributions have some detailed differences in the polar cap and nightside regions.

Including the electric field variability into the energy calculation results in significant changes to the neutral temperature and density. For example, it causes a 120 K polar average exospheric temperature increase at 400 km ranging from 62 K to 250 K. The corresponding percentage difference of density is close to 30% for the polar average, and the localized difference can be 16% to 75%.

Acknowledgments.

National Center for Atmospheric Research (NCAR) is supported by National Science Foundation (NSF). This research was supported by the NASA Living With a Star grant NNH05AB54I and the AFOSR Contract FA9550-08-C-0046.

189 The editor thanks both of the referees for their assistance in evaluating this paper.

References

190 Codrescu, M. V., T. J. Fuller-Rowell, and J. C. Foster, On the importance of E-field variability
191 for Joule heating in the high-latitude thermosphere, *Geophys. Res. Lett.*, *22*, 2393, 1995.

192 Codrescu, M. V., T. J. Fuller-Rowell, J. C. Foster, J. M. Holt, and S. J. Cariglia, Electric field
193 variability associated with the Millstone Hill electric field model, *J. Geophys. Res.*, *105*, 5265,
194 2000.

195 Crowley, G., and C. L. Hackert, Quantification of high latitude electric field variability, *Geo-*
196 *phys. Res. Lett.*, *28*, 2783, 2001.

197 Deng, Y., A. Maute, A. D. Richmond, and R. G. Roble, Analysis of thermospheric response
198 to magnetospheric inputs, *Journal of Geophysical Research (Space Physics), 113*, doi:
199 10.1029/2007JA012840, 2008.

200 Emery, B. a., C. Lathuillere, P. G. Richards, R. G. Roble, M. J. Buonsanto, D. J. Knipp,
201 P. Wilkinson, D. P. Sipler, and R. Niciejewski, Time dependent thermospheric neutral re-
202 sponse tothe 2-11 November 1993 storm period, *Journal of Atmospheric and Terrestrial*
203 *Physics*, *61*, 329–350, 1999.

204 Fesen, C. G., B. A. Emery, M. J. Buonsanto, Q. H. Zhou, and M. P. Sulzer, Simulations of
205 the F region during the January 1993 10-day campaign, *J. Geophys. Res.*, , *102*, 7249–7266,
206 doi:10.1029/96JA03312, 1997.

207 Foster, J. C., J. M. Holt, R. G. Musgrove, and D. S. Evans, Ionospheric convection associated
208 with discrete levels of particle precipitation, *Geophys. Res. Lett.*, *13*, 656, 1986.

Fuller-Rowell, T. J., and D. Evans, Height-integrated Pedersen and Hall conductivity patterns inferred from TIROS–NOAA satellite data, *J. Geophys. Res.*, *92*, 7606, 1987.

Hardy, D. A., M. S. Gussenhoven, R. Raistrick, and W. J. McNeil, Statistical and fuctional representation of the pattern of auroral energy flux, number flux, and conductivity, *J. Geophys. Res.*, *92*, 12,275, 1987.

Liu, H., H. Lühr, V. Henize, and W. Köhler, Global distribution of the thermospheric total mass density derived from CHAMP, *Journal of Geophysical Research (Space Physics)*, *110*, 4301–+, doi:10.1029/2004JA010741, 2005.

Matsuo, T., and A. D. Richmond, Effects of high-latitude ionospheric electric field variability on global thermospheric Joule heating and mechanical energy transfer rate, *Journal of Geophysical Research (Space Physics)*, *113*, 7309–+, doi:10.1029/2007JA012993, 2008.

Matsuo, T., A. D. Richmond, and K. Hensel, High-latitude ionospheric electric field variability and electric potential derived from DE-2 plasma drift measurements: Dependence on IMF and dipole tilt, *J. Geophys. Res.*, *108*, 1005, 2003.

Richmond, A. D., Assimilative mapping of ionospheric electrodynamics, *Adv. Space Res.*, *12*, 59, 1992.

Ridley, A. J., G. Crowley, and C. Freitas, A statistical model of the ionospheric electric potential, *Geophys. Res. Lett.*, *27*, 3675, 2000.

Roble, R. G., E. C. Ridley, A. D. Richmond, and R. E. Dickinson, A coupled thermosphere/ionosphere general circulation model, *Geophys. Res. Lett.*, *15*, 1325, 1988.

Ruohoniemi, J. M., and R. A. Greenwald, Statistical patterns of the high-latitude convection obtained from Goose Bay HF radar observations, *J. Geophys. Res.*, *101*, 21,743, 1996.

231 Thayer, J. P., and J. F. Vickrey, On the contribution of the thermospheric neutral wind to high-
232 latitude energetics, *Geophys. Res. Lett.*, *19*, 265, 1992.
233 Weimer, D. R., An improved model of ionospheric electric potentials including substorm pertur-
234 bations and application to the Geosphace Environment Modeling November 24, 1996, event,
235 *J. Geophys. Res.*, *106*, 407, 2001.
236 Weimer, D. R., Improved ionospheric electrodynamic models and application to calculating
237 Joule heating rates, *Journal of Geophysical Research (Space Physics)*, *110*, 5306–+, doi:
238 10.1029/2004JA010884, 2005.

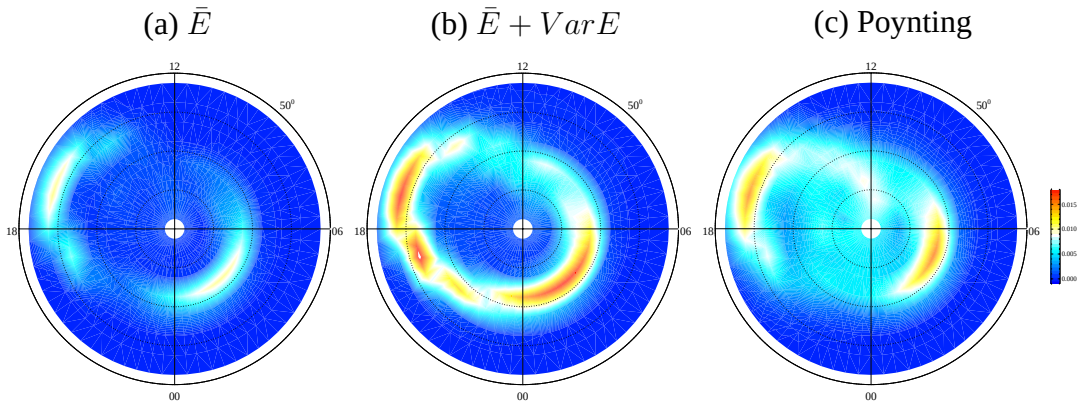

Figure 1. (a) Distribution of the altitude-integrated Joule heating from a TIEGCM simulation, when the average electric field is used in the Joule heating calculation. The IMF conditions are $B_y = 0$ and $B_z = -5nT$. The hemispheric power is 30 GW and $F_{10.7}$ is $150 \times 10^{-22} W/m^2 Hz$. Geographic coordinates are used in this figure. (b) Same as (a), but the electric field variability from the empirical model is also included in the calculation. (c) Poynting flux at the top of the thermosphere from the empirical model.

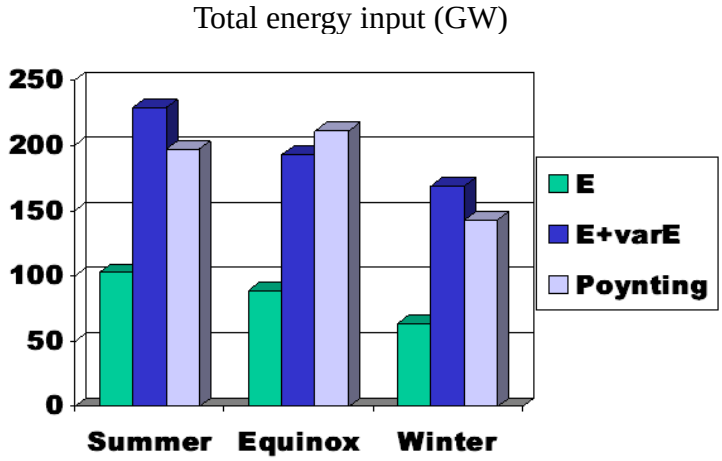

Figure 2. Hemispherically integrated Joule heating from TIEGCM simulations and Poynting flux from the empirical model in different seasons. The green columns are for the case in which the average electric field is used in the Joule heating calculation. The dark blue columns are for the case in which both average electric field and electric field variability are included in the calculation. The light blue columns represents the integrated Poynting flux from the empirical model.

(a) Polar average T_n

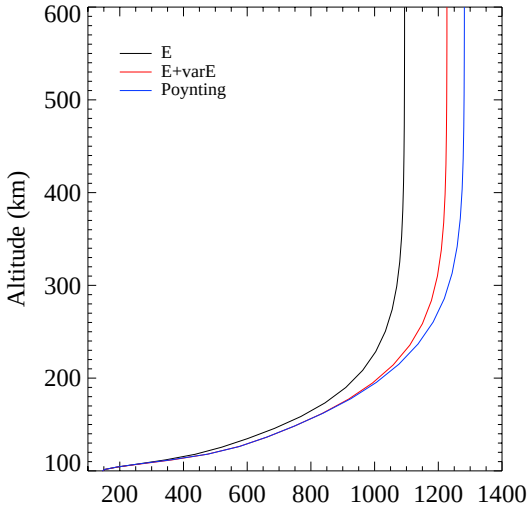

(b) Distribution of temperature difference at 400 km

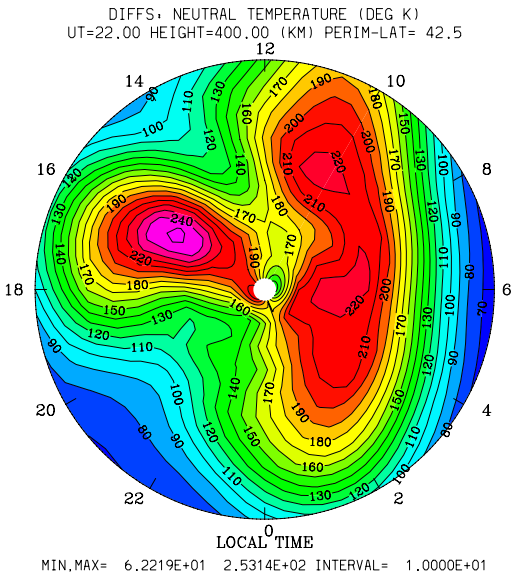

Figure 3. (a) Polar average (poleward 47.5°) thermospheric temperature profiles at equinox with different high-latitude energy inputs. The black line is for the case in which Joule heating is calculated with the average electric field. The red line is for the case in which both the average electric field and electric field variability are included in the Joule heating calculation. The blue line is for the case in which the energy input is specified by the Poynting flux from the empirical model (see text). (b) Distribution of temperature difference between the cases with and without the electric field variability at 400 km altitude.

(a) Percentage difference of polar average density

(b) Distribution of density percentage difference at 400 km

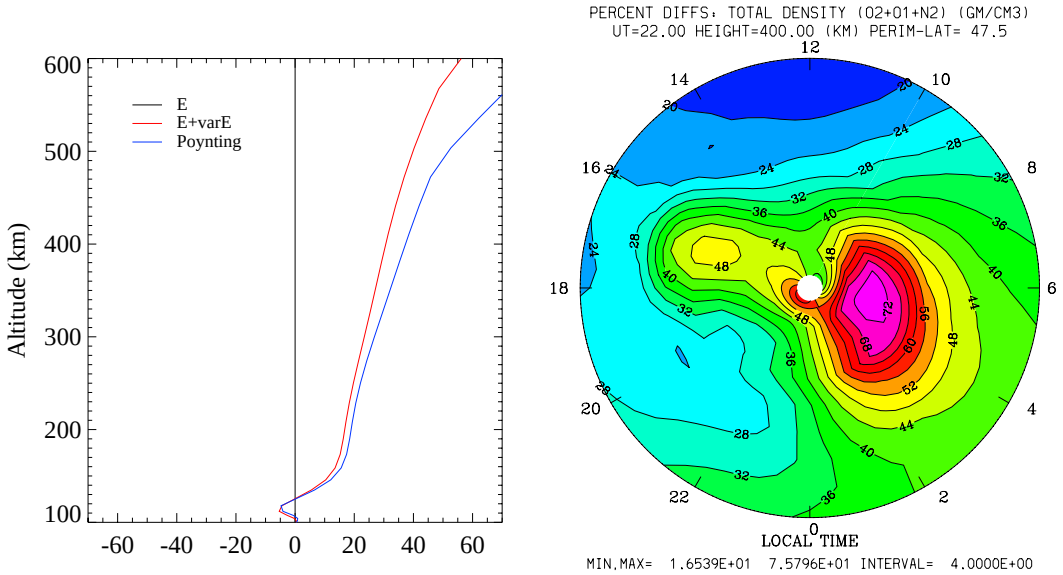

Figure 4. (a) Percentage difference of the polar average (poleward 47.5°) thermospheric density compared with the average electric field case. The black line is for the case in which Joule heating is calculated with the average electric field. The red line is for the case in which both the average electric field and electric field variability are included in the Joule heating calculation. The blue line is for the case in which the energy input is specified by the Poynting flux from the empirical model. (b) Distribution of percentage density difference between the cases with and without the electric field variability at 400 km altitude.